ELECTRONIC SUPPLEMENTARY INFORMATION

A New Approach for Crystallization of Copper(II) Oxide Hollow Nanostructures with Superior Catalytic and Magnetic Response

Inderjeet Singh,[1,2] Katharina Landfester,[2]

Amreesh Chandra,[1,*] and Rafael Muñoz Espí[2,3*]

[1]Department of Physics, Indian Institute of Technology, Kharagpur – 721302, West Bengal, India

[2]Max Planck Institute for Polymer Research, Ackermannweg 10, 55128 Mainz, Germany

[3] Institute of Materials Science (ICMUV), University of Valencia, PO Box 22085, 46071 Valencia, Spain.

Contents

1. X-ray Diffraction Pattern of CuO After Densification

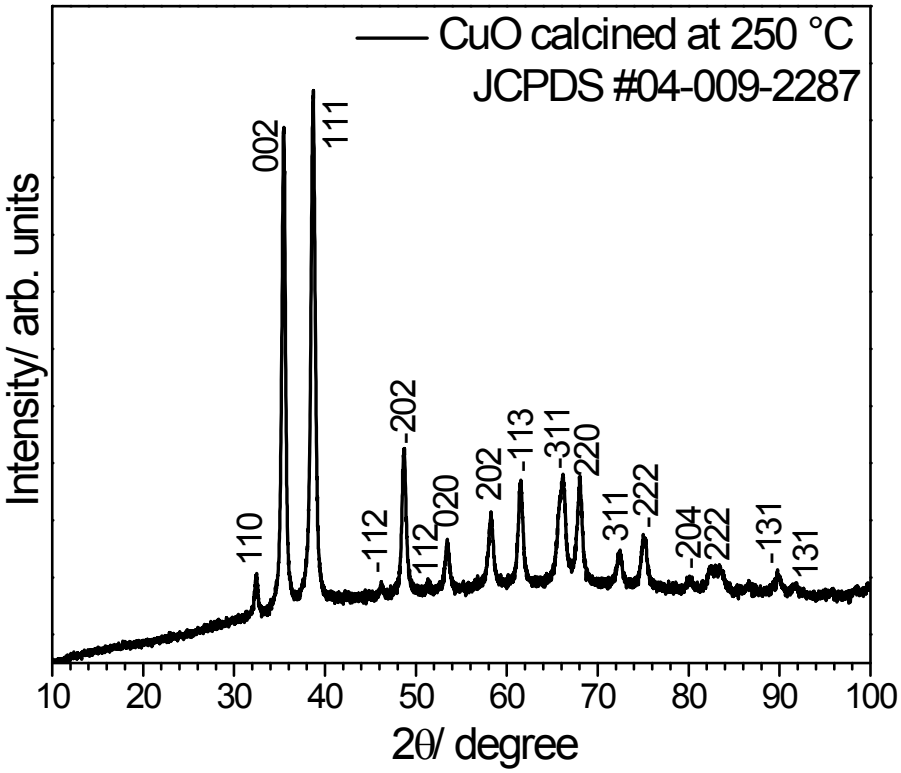

Fig. S1: XRD pattern of CuO powders calcined at 250 ^{o}C.

2. X-ray Photoelectron Spectroscopy Measurements

X-ray Photoelectron Spectroscopy Measurements (X-ray Photoelectron Spectroscopy Analysis)

Fig. S2 shows the X-ray photoelectron spectroscopy (XPS) data. This technique was used to examine the chemical composition and oxidation states of Cu and O in hollow CuO powders. The complete survey scan of powders shown in Fig. S2(a) confirms the presence of Cu and O in the powders along with presence of carbon, which can get adsorbed on to the powders. The XPS core level spectrum of Cu $2p_{3/2}$ is shown in Fig. S2(b). Peak for Cu $2p_{3/2}$ can be fitted well with a single Gaussian contribution arising at 933.6 eV. This confirms the presence of only Cu^{2+} oxidation state in the sample. Peaks observed at 933.6 and 953.6 eV in Cu 2p core level spectra correspond to Cu $2p_{3/2}$ and Cu $2p_{1/2}$.[1] The values of binding energy for Cu $2p_{3/2}$ and Cu $2p_{1/2}$ matches closely with reported data.[2] Distance of ~20 eV between two peaks also corresponds to standard spectra of Cu 2p.[7] The XPS core level spectrum of O1s is shown in Fig. S2(c). The O1s spectrum can be fitted using two peaks as shown in the Fig. S2(c). These two peaks arise at 529.5 and 530.6 eV. Peak observed at a lower binding energy of 529.5 eV is due to presence of O^{2-} in Cu-O bond.[3] Other peak at higher binding energy of 530.6 eV can be attributed to the presence of chemically adsorbed oxygen on to the surface of CuO.[1, 3]

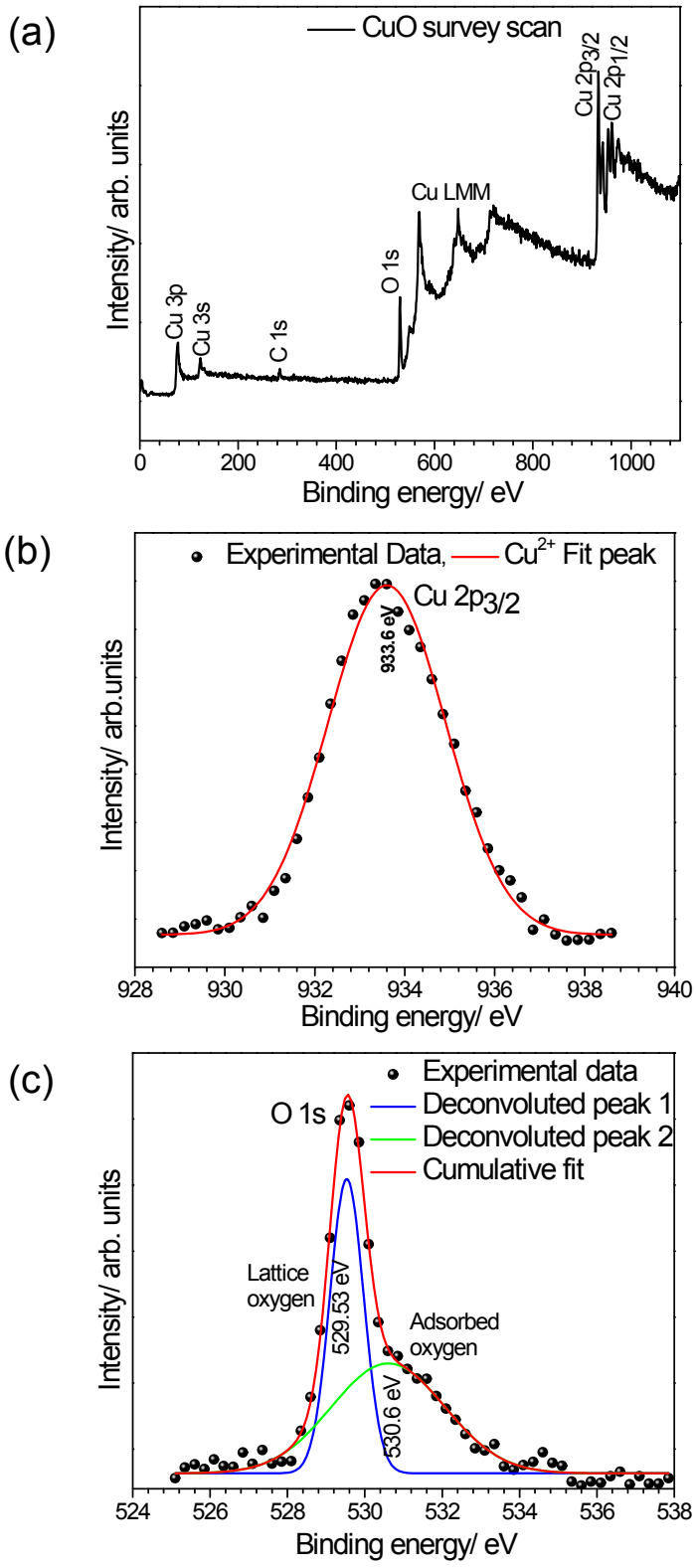

Fig. S2: X-ray photoelectron spectroscopy data of hollow CuO showing (a) sample survey scan, and peak profile fittings of (b) core level Cu2p spectrum, and (c) core level O1s spectrum.

3. Morphology Characterization

3.1 Effect of Reaction Temperature and Precursor Concentration

Fig. S3 shows the morphology analysis of the samples precipitated at room temperature. Fig. S3(a) shows the TEM image of CuO structures using PIBSP and triethylamine (TEA) with the precursor [$Cu(NO_3)_2 \cdot 3H_2O$] concentration of 0.5 M. TEM images clearly show that the hollow morphologies, formed by entanglement of rod-like particles at the interface of the droplet, are also observed at room temperature. Fig. S3(b) shows the image of the hollow structures at higher magnification. The results confirm that the increase of the temperature in the emulsions does not significantly affect the kinetics of the interfacial precipitation of the precursor species. Fig. S3(c) and S3(d) show TEM images using higher precursor concentrations (1 M and 2 M, respectively). In this case also, precipitated particles possess the same hollow morphologies, following a similar growth mechanism.

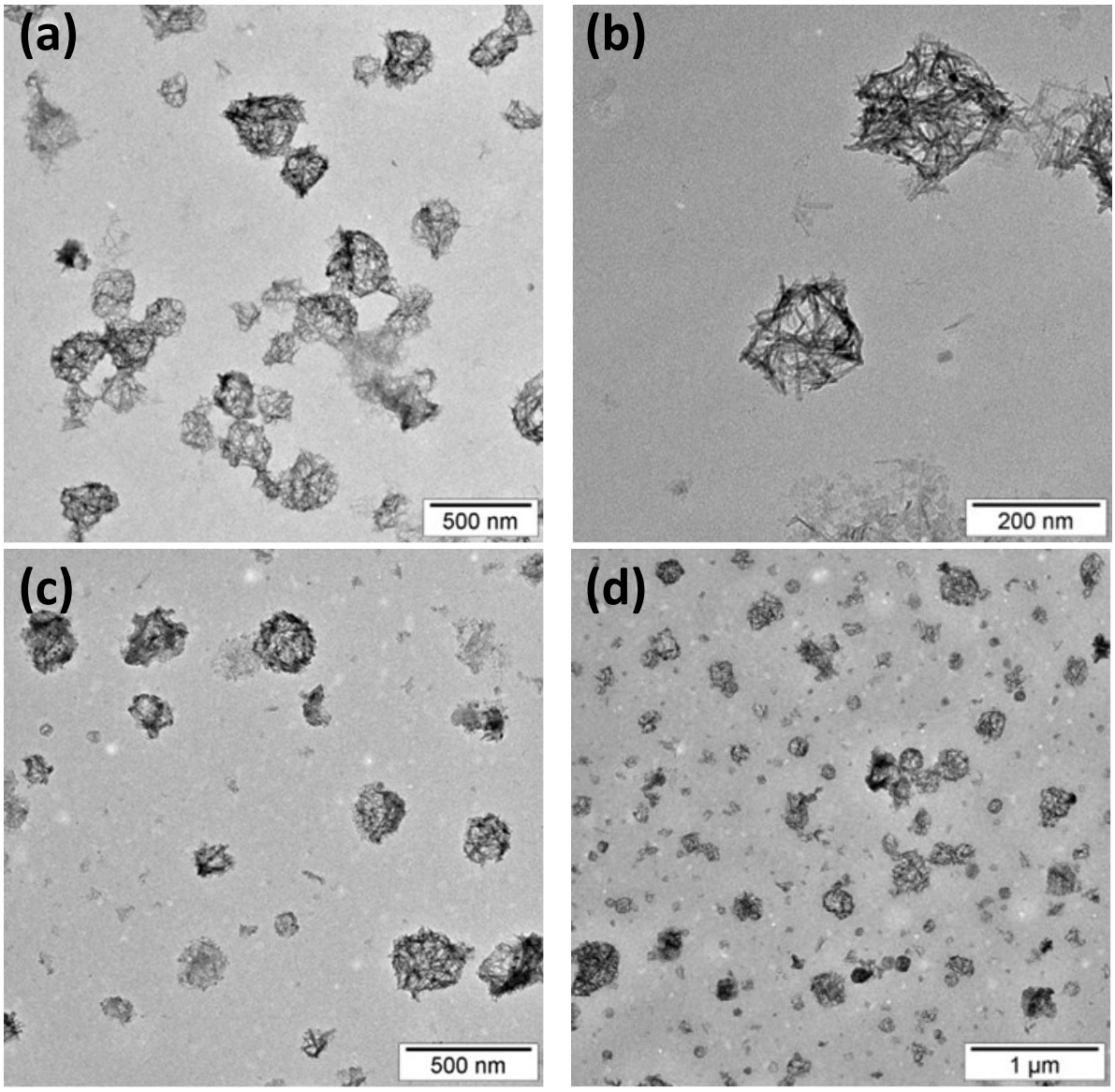

Fig. S4: TEM images of the samples prepared at room temperature using TEA and PIBSP with precursor concentration of (a) 0.5 M, (b) image with higher magnification for 0.5 M, (c) 1 M, and (d) 2 M.

3.2 Effect of the Surfactant

To confirm the role of amine groups for the formation of hollow nanostructures, sythesis of CuO was performed using PGPR (polyglycerol polyricinoleate)—which does not have amine groups attached—as a surfactant while keeping the other reaction conditions constant (precursor concentration: 0.5 M, precipitating agent: trimethylamine (TEA), reaction temperature: 80 ^{o}C). Fig. S4 shows the TEM micrograph of CuO prepared using PGPR as a surfactant. In this case, precipitation of the precursor species at the droplet interface could not be obtained upon addition of TEA, and rod like morphologies of CuO was observed. This result is consistent with the absence of the complexation of Cu(II) ions at the droplet interface when using PGPR as a surfactant. Accordingly, amine groups of the PIBSP surfactant play a major role in achieving hollow morphologies of CuO, as discussed in the formation mechanism of hollow nanostructures.

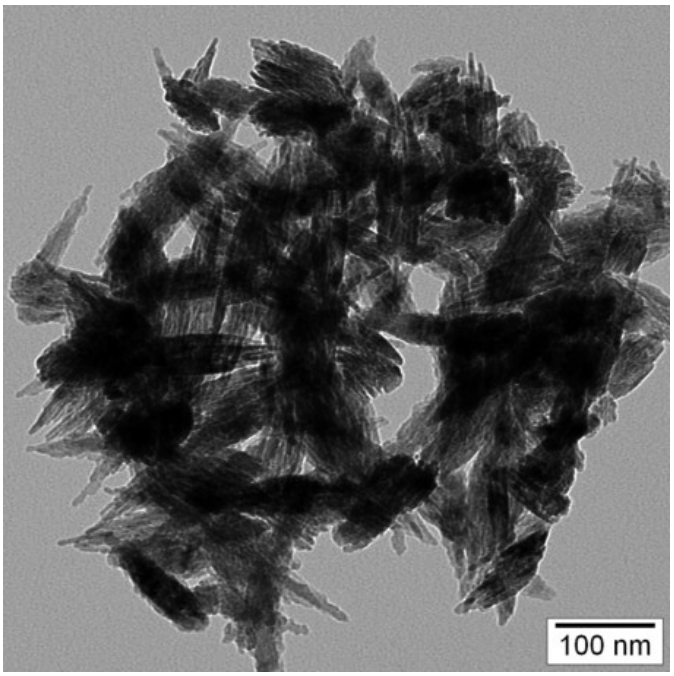

Fig. S4: TEM image of the samples prepared at 80 ^{o}C using TEA and PGPR with precursor concentration of 0.5 M.

4. Adsorption–Desorption Measurements

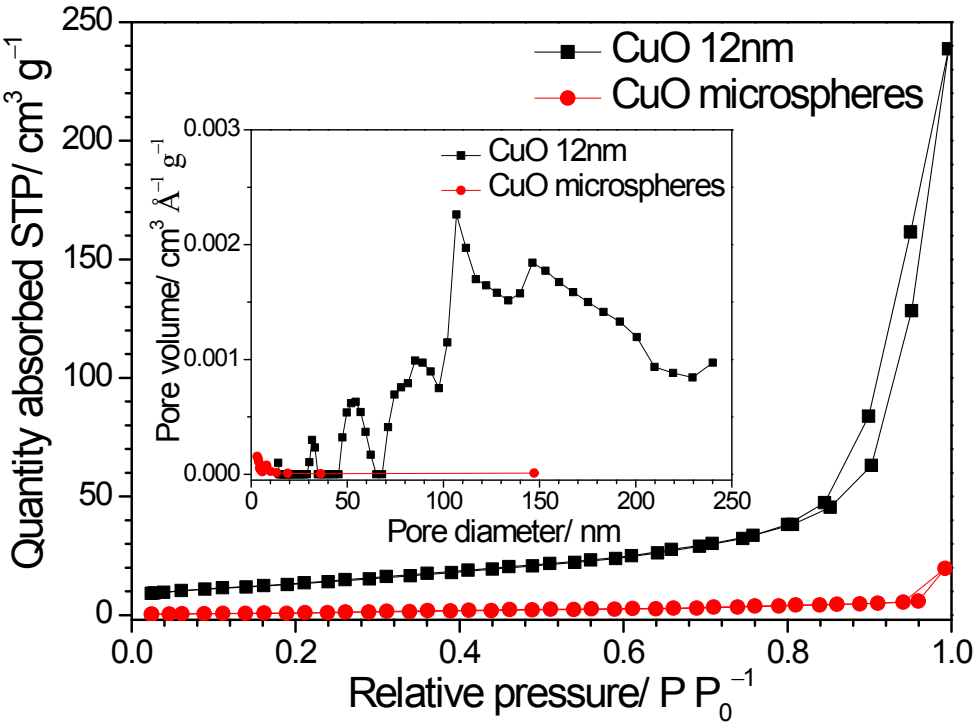

Fig. S5: Adsorption–desorption measurements for 12-nm CuO particles and CuO microspheres

5. Catalytic activity Measurements of CuO Microspheres and 12-nm Particles

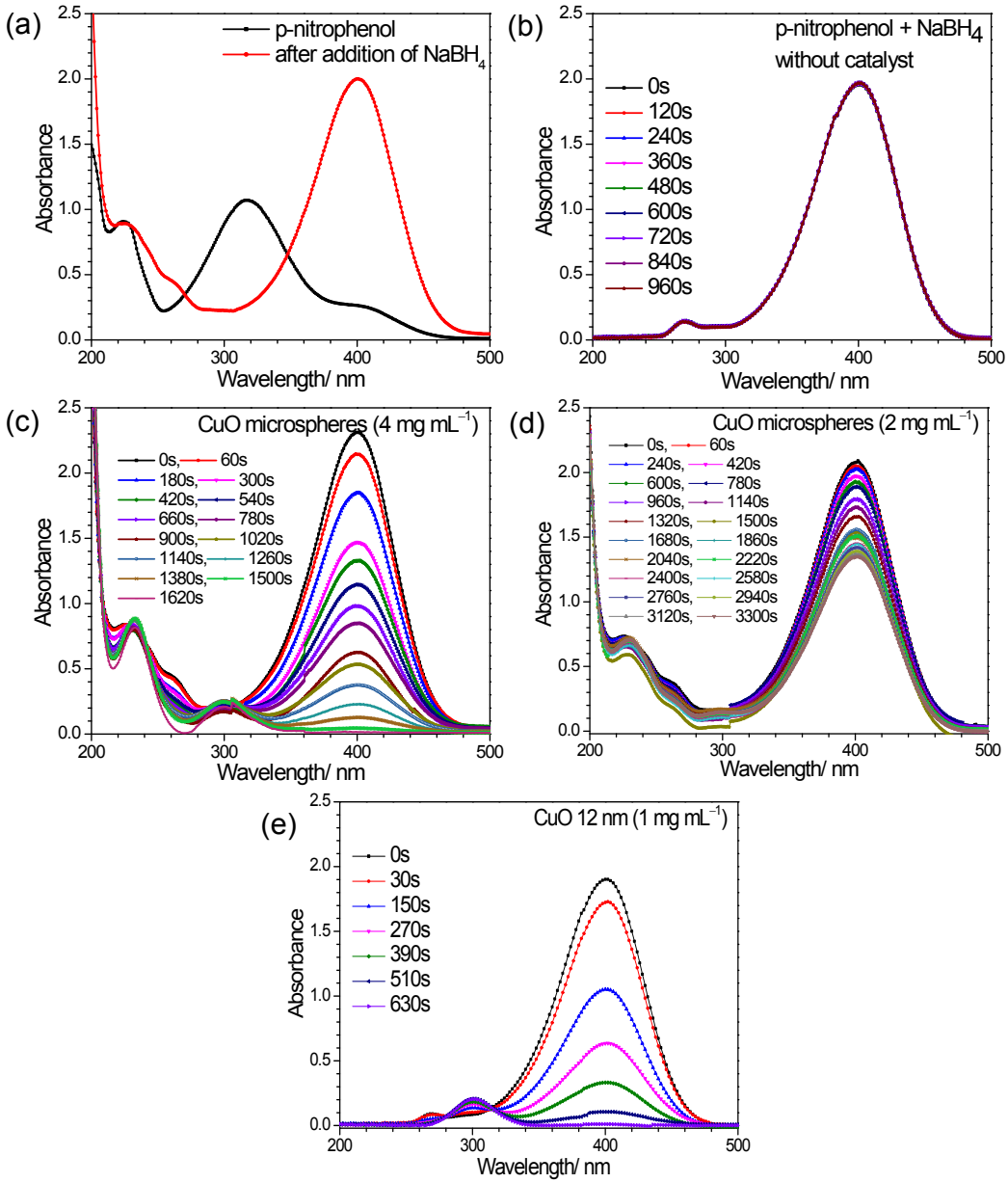

Fig. S6: (a) UV-Vis spectra of *p*-nitrophenol aqueous solution and after addition of $NaBH_4$, (b) UV-Vis spectra for *p*-nitrophenol reduction without a catalyst, (c) UV-Vis spectra for *p*-nitrophenol reduction using commercial CuO powders in bulk at a concentration of 4 mg mL^{-1}, (d) UV-Vis spectra for *p*-nitrophenol reduction using commercial CuO powders in bulk at a concentration of 2 mg mL^{-1}, and (e) UV-Vis spectra for *p*-nitrophenol reduction using 12-nm CuO powders at a concentration of 1 mg mL^{-1}.

6. Recycling Activity Tests for Hollow CuO Nanostructures

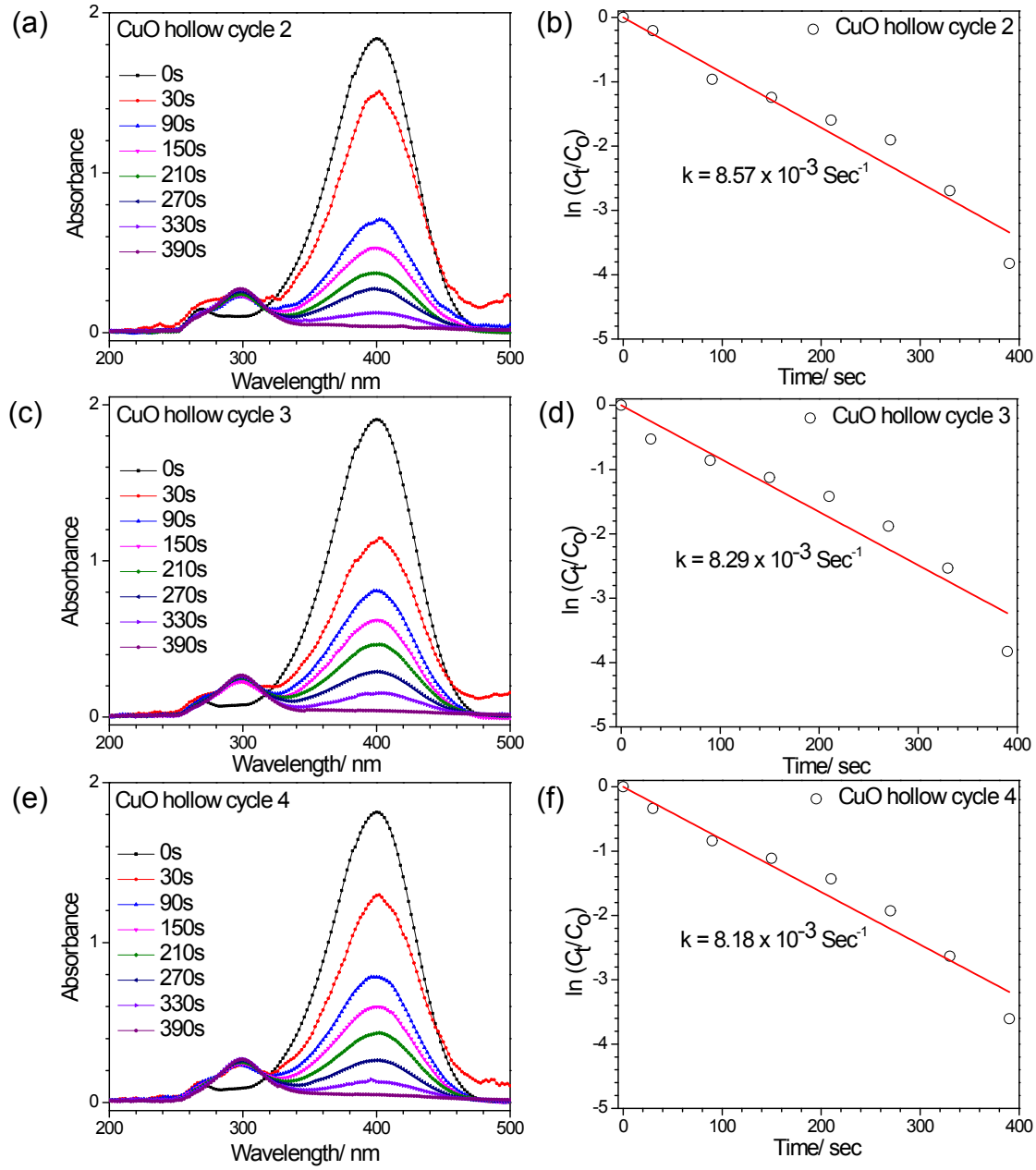

Fig. S7: (a, c, e) UV-Vis spectra of the powders for *p*-nitrophenol reduction catalyzed using hollow CuO in cycle 2,3 and 4, (b, d, f) variation of ln(Ct/C_0) with time for calculation of reaction rate constants.

7. X-ray Diffraction Pattern Comparison for CuO Powders after Recycling Tests

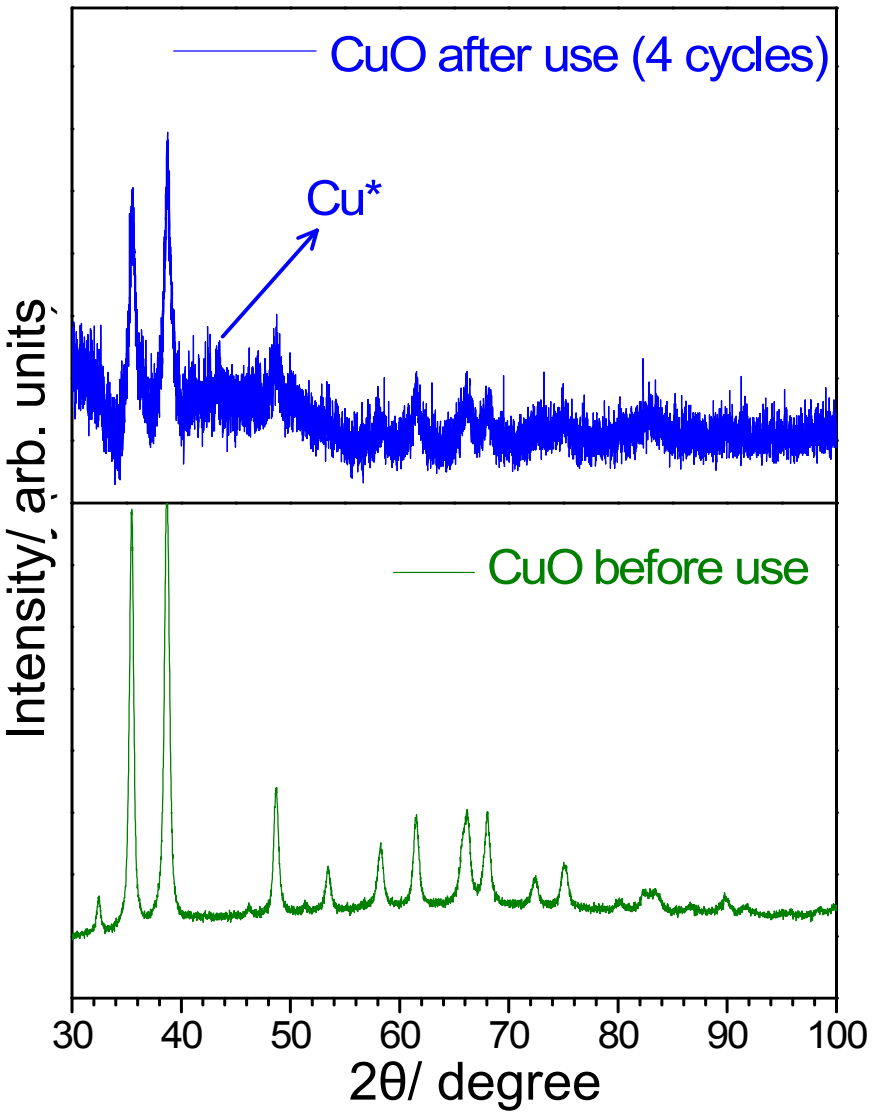

Fig. S8: Comparison of XRD pattern of CuO powders used for catalysis before usage and after usage of 4 cycles.

8. Magnetic Measurements of CuO Microspheres

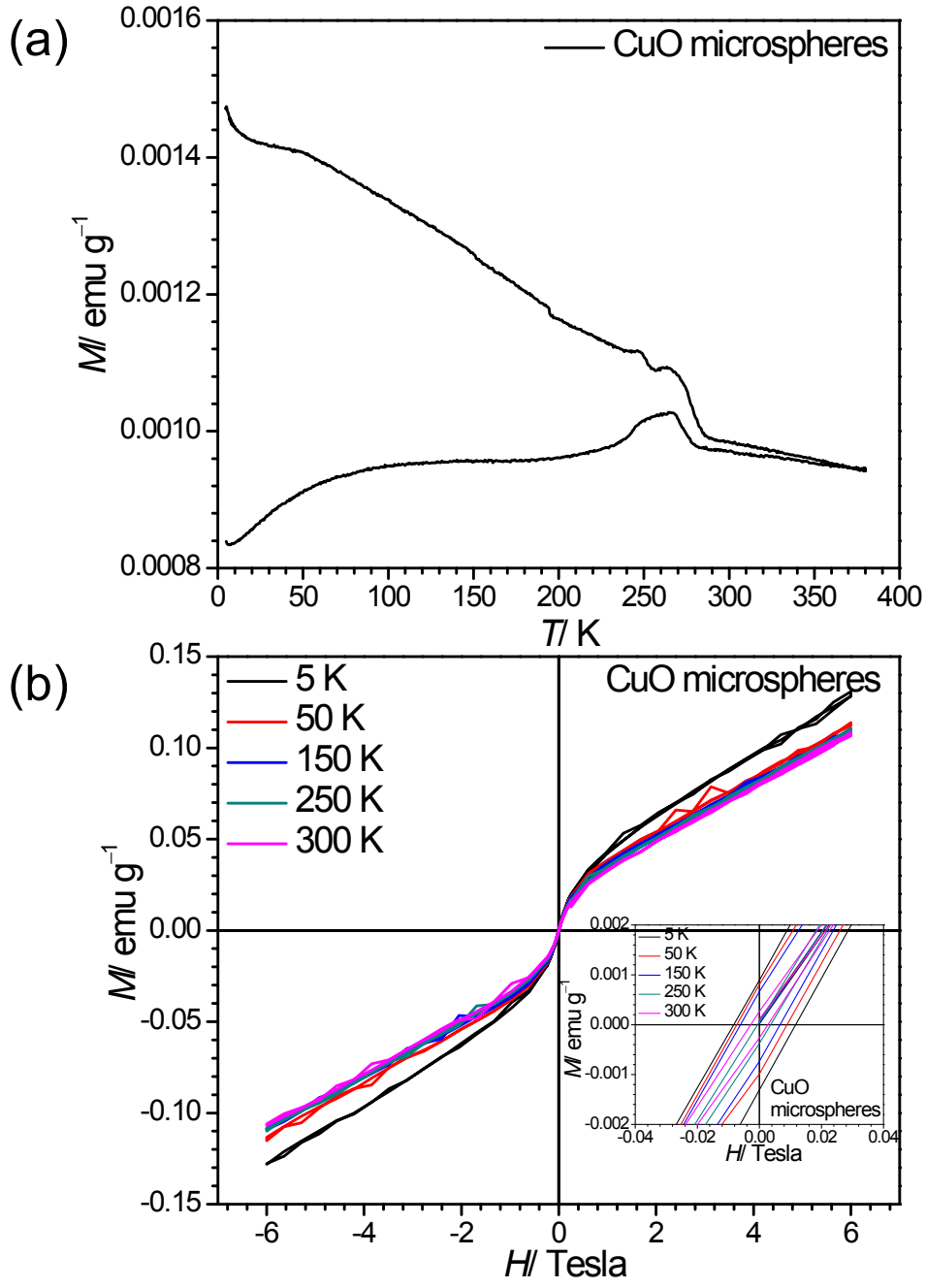

Fig. S9: (a) ZFC-FC curves at 100 Oe and (b) M-H curves at 5 K, 50 K, 150 K, 250 K and 300 K for commercial CuO microspheres.

9. Comparison of Catalytic Activity of Hollow CuO with Previous Works

Table S1: Comparison of different metal and metal oxide based catalysts used for *p*-nitrophenol reduction

No.	Catalyst	Morphology	Concentration of *p*-nitrophenol (M)	Rate Constant (s^{-1})	References
1	Pd/AAO	Nanowire array	0.94×10^{-4}	6.7×10^{-3}	[4]
2	PPy/TiO_2/Pd	Nanofiber composite	0.86×10^{-4}	12.2×10^{-3}	[5]
3	Pd	Nanocrystals	0.8×10^{-4}	4.83×10^{-3}	[6]
4	Ag	Coral like dendrite	1×10^{-4}	5.19×10^{-3}	[7]
5	Au	Spongy	1.03×10^{-4}	2.1×10^{-3}	[8]
6	Pd-CeO_2	Nanoparticles	0.5×10^{-4}	17.1×10^{-3}	[9]
7	CuO	Hollow	1×10^{-4}	12.63×10^{-3}	This work

References:

1. M. A. Dar, Y. S. Kimb, W. B. Kima, J. M. Sohnc and H. S. Shin, *Appl. Surf. Sci.*, 2008, **254**, 7477-7481.
2. M. Basu, A. K. Sinha, M. Pradhan, S. Sarkar, A. Pal and T. Pal, *Chem. Commun.*, 2010, **46**, 8785-8787.
3. W.-T. Yao, S.-H. Yu, Y. Zhou, J. Jiang, Q.-S. Wu, L. Zhang and J. Jiang, *J. Phys. Chem. C*, 2005, **109**, 14011-14016.
4. R. Li, P. Zhang, Y. Huang, C. Chen and Q. Chen, *ACS Appl. Mater. Interfaces*, 2013, **5**, 12695-12700.
5. X. Lu, X. Bian, G. Nie, C. Zhang, C. Wang and Y. Wei, *J. Mater. Chem.*, 2012, **22**, 12723.
6. G. Fu, X. Jiang, L. Ding, L. Tao, Y. Chen, Y. Tang, Y. Zhou, S. Wei, J. Lin and T. Lu, *Appl. Catal. B*, 2013, **138-139**, 167-174.
7. M. H. Rashid and T. K. Mandal, 2007, **111**, 16750-16760.
8. M. H. Rashid, R. R. Bhattacharjee, A. Kotal and T. K. Mandal, *Langmuir*, 2006, **22**, 7141-7143.
9. J. Liu, W. Wang, T. Shen, Z. Zhao, H. Feng and F. Cui, *R. Soc. Chem. Adv.*, 2014, **4**, 30624.